Nanoparticle-based plasmonic organic photovoltaic devices

Emmanuel Stratakis[1,*] and Emmanuel Kymakis[2,*]

[1] Institute of Electronic Structure and Laser (IESL), Foundation for Research and Technology-Hellas (FORTH), Heraklion, 71110 Crete, Greece
[2] Center of Materials Technology & Photonics and Electrical Engineering Department, Technological Educational Institute (TEI) of Crete, Heraklion, 71004 Crete, Greece

Plasmonic metallic nanoparticles (NPs) have recently been identified as a breakthrough route for enhancing the efficiency of organic photovoltaic (OPV) devices. The present review highlights the different strategies of incorporating plasmonic NPs for light trapping into either the active or the buffer layer or at various interfaces within the OPV cell architecture. In addition, it summarizes the different enhancement mechanisms that have been proposed and indicates future trends in the development of NPs-based solution processable OPVs. The aim is to distinguish among the different plasmonic effects and to propose potential strategies for performance optimization.

Introduction

The ongoing financial crisis combined with recent world events in countries with large fossil fuel reserves has clearly demonstrated the need for the rapid development of a low cost, large scale and 'green' energy technology. In this concept, solar energy through photovoltaic energy conversion is the most promising candidate for long term sustainable energy production. Organic photovoltaics (OPVs) hold the promise for a cost-effective, lightweight solar energy conversion platform particularly for the provision of off-grid electricity [1] and portable consumer electronics [2], which can benefit from simple solution processing of the active layer at room temperatures [3]. One highly successful OPV design concept is based on the polymer–fullerene bulk heterojunction (BHJ) type of devices, which is characterized by a complex interpenetrating network of the two phases, where power conversion efficiencies (PCEs) of over 8% have been reported [4,5]. The commercialization of OPVs can spark into life once the efficiencies for single junction devices exceed 10%.

A major hindrance toward the development of OPVs is the fundamental tradeoff between light absorption and collection of photogenerated excitons. Efficient charge transport in BHJ OPVs is achieved provided that continuous pathways for both charge carriers exist. Naturally, the presence of such pathways is less likely for

thicker active layers. In addition, carriers exhibit reduced exciton diffusion lengths in organic semiconductors due to limited hopping transport [6]. As a result, active layer thicknesses in optimized OPV devices are small, typically around 200 nm. Owing to such a low active layer thickness, the best devices that have been developed absorb poorly, despite displaying low charge–carrier recombination. Fig. 1 summarizes the number of photons (N_{ph}) absorbed and J_{sc} in the most studied BHJ system, namely a P3HT:PCBM layer, versus the thickness of this blend for an optimized organic solar cell structure. [7] It shows that, despite the fact that the theoretical J_{sc} of a P3HT:PCBM blend could be close to 19 mA cm^{-2}, the practically achievable value of real devices will be in the range of 10–12 mA cm^{-2}. Therefore, enhancement of the absorbance of a polymer film of a specific limited thickness still remains a challenge. Research in this area has indicated that the compromise between efficient light harvesting and efficient charge collection, determined by the organic layer thickness, can be resolved by 'trapping' incident light in the active layer.

One promising plasmon enhanced light-trapping approach is the utilization of plasmonic metallic nanoparticles (NPs) either between interfaces, or inside the buffer or the active layers of OPV devices in order to promote absorption, thereby increasing the optical thickness of OPV materials for light harvesting [8,9]. Noble metallic NPs are known to exhibit a strong absorption band in the UV–Vis region, which lies within the optical absorption band of the conjugated polymers used in the active layer of OPVs. The

*Corresponding authors:. Stratakis, E. (stratak@iesl.forth.gr),
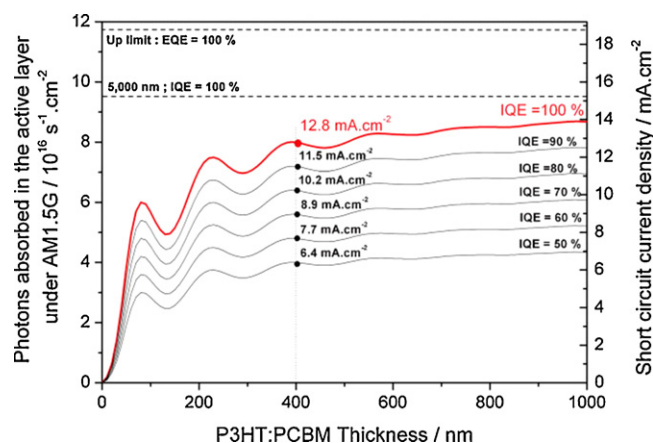Kymakis, E. (kymakis@staff.teicrete.gr)

1369-7021/06 © 2013 Elsevier Ltd. http://dx.doi.org/10.1016/j.mattod.2013.04.006 **133**

FIGURE 1

Number of photons (N_{ph}) absorbed in the active layer under AM1.5G calculated by transfer-matrix formalism (TMF), for a device having the following structure: glass (1 mm)/ITO (140 nm)/PEDOT:PSS (50 nm)/P3HT:PCBM (values in x-axis nm)/Al(100 nm). The right axis represents the corresponding short circuit current (J_{sc}) at various IQEs, indicated in the graph. Reprinted with permission from Ref. [7] © 2009 John Wiley & Sons, Inc.

physical origin of this enhanced absorption is the coherent oscillation of the free electrons, coined as a plasmon wave, which is excited by the incident electromagnetic field [10]. When the electron cloud is displaced relative to the nuclei, a restoring force arises from Coulomb attraction between electrons and nuclei that results in an oscillation of the electron cloud relative to the nuclei framework. For NPs with dimensions well below the wavelength of light in the quasi-static limit, the scattering and absorption cross-sections are given by [11]

$$\sigma_{sc} = \frac{1}{6\pi}\left(\frac{2\pi}{\lambda}\right)^4 |a|^2, \quad \sigma_{abs} = \frac{2\pi}{\lambda} \, \text{Im}[a]$$

where $a = 3V((\varepsilon_p/\varepsilon_m) + 1)/((\varepsilon_p/\varepsilon_m) + 2)$ is the polarizability of the particle. Here V is the particle volume, ε_p is the dielectric function of the particle and ε_m is the dielectric function of the embedding medium. The scattering efficiency Q_{sc} is given by $Q_{sc} = \sigma_{sc}/(\sigma_{sc} + \sigma_{abs})$ [12]. We can see that when the light frequency is such that $\varepsilon_p = -2\varepsilon_m$ the particle polarizability and the absorption cross section become maximal (resonance) and this condition is termed the localized surface plasmon resonance (LSPR, non-propagating excitations of conduction electrons within a metallic nanostructure). The LSPR frequency depends on the size and shape of the NP, the NP material and the optical constants of the NP surrounding medium [13].

From the above equations, it is clear that NPs act as local field enhancers or light scattering centers or both, depending on their size [9,11,15]. Absorption dominates for small NPs with diameters in the range 5–20 nm. In this case NPs behave as subwavelength antennas, due to LSPR excitation (Fig. 2(b)). The plasmonic near-field is coupled to the photoactive layer, increasing its effective absorption cross-section and thus exciton dissociation. On the other hand, relatively larger diameter (>50 nm) NPs behave as effective subwavelength scattering elements that couple and trap freely propagating plane waves of the incident light into the photoactive layer (Fig. 2(a)) [16]. At LSPR, such NPs can have a scattering cross-section much larger than their geometric cross-section [11]. In this case, enhanced absorption takes place by an increase of the optical path length inside the photoactive layer, caused by the light being reemitted in different directions within the device.

Finally, NPs can be placed in the form of a periodically arranged nanoarray at the front or back contact of OPV devices (Fig. 2(c)). In this case, incident light can excite resonant scattering modes coined as surface plasmon polaritons (SPP) at each individual NP-active layer interface. Depending on the NP shape, various modes can be excited, attributed to geometric resonances of SPPs
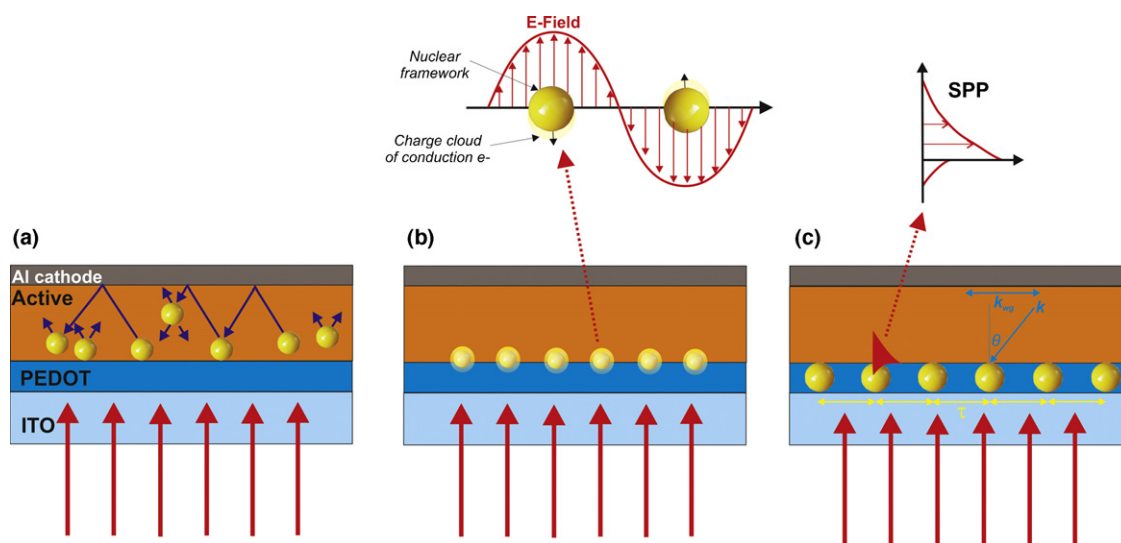

FIGURE 2

(Top) Schematic of the plasmon oscillation of a sphere, showing the displacement of the conduction electrons relative to the nuclei [14]. (Bottom) Different geometries for plasmonic light trapping in OPVs: (a) scattering from large diameter (>50 nm) metal NPs into high angles inside the photoactive layer, causing increased optical path lengths in the device; (b) LSPRs induced by small diameter (5–20 nm) metal particles and (c) excitation of SPPs at the NPs/photoactive layer interfaces ensures the coupling of incident light to photonic modes propagating in the semiconductor layer plane. The 2D periodic array of NPs scatterers could also provide in-plane momentum for scattered light to be coupled into waveguide modes (see text).

at the NPs-layer interface [17]. In addition, a 2D array of NPs scatterers could provide momentum in the in-plane direction for scattered light to be coupled into propagation or waveguide modes [18,19]. Such modes propagate along the NP-active layer interface resulting in the absorption enhancement of the latter (Fig. 2(c)). The collective scattering from the particle array will result into different diffraction orders, q, that each scatter at a different angle. The in-plane momentum generated by a grating with pitch τ is given by $q2\pi/\tau$ with $q = \pm1$, ±2, ±3, ... The requirement for coupling to the waveguide mode is that its momentum, k_{wg}, equals the in-plane momentum of the incoming light, $k \sin \vartheta$, plus that provided by the grating (see Fig. 2(c)).

$$k_{wg} = k \sin \vartheta + q \frac{2\pi}{\tau}$$

The principle of momentum matching, thus states that light can couple to waveguide modes under the conditions given by the equation above. As several modes are supported in the waveguide (the different modes are directly determined by the NP geometry and the waveguide thickness) and because multiple grating orders can contribute to the momentum matching, in practice many combinations of k–θ fulfill the equation. Therefore, the geometrical parameters of nanoarrays, including the period, NP height and width, must be carefully designed to achieve the optimum momentum transfer and in turn absorption enhancement.

At the same time, recent research efforts have revealed that the dispersion of NPs into the photoactive layer leads to an improvement of its structural stability, giving rise to slower device degradation rate upon prolonged illumination [20]. Therefore, the performance enhancement can also be attributed to the improvement of the blend as well as the electrode–blend interface morphology due to the presence of NPs. Overall, the incorporation of metallic NPs in the active layer could lead to performance enhancement via two processes; a light harvesting effect causing improved initial cell efficiency and an improved structural stability effect giving rise to superior device durability.

This review article addresses recent advances in the rapidly developing field of plasmonic organic photovoltaics. Metallic NPs of various sizes, shapes and configurations have been integrated into OPV cell architecture in order to tune and enhance, in a wavelength-dependent manner, the optical absorption of respective devices. As a result impressive improvements in the respective device efficiencies were achieved. The incorporation of NPs in OPV devices can be classified into three major classes, depending on their position in the solar cell architecture (Fig. 3): NPs dispersed into the (i) photoactive and (ii) buffer layers as well as (iii) between different interfaces [18]. Such classes are fundamentally different in terms of absorption and performance enhancement mechanisms. Table 1 summarizes the state of the art reports on plasmon NP-based OPV devices indicating the respective efficiency improvements.

Synthesis of plasmonic metallic NPs

Metal NPs have been used in decorative pigments since the time of the Romans when it was discovered that silver and gold particles at the nanoscale exhibit unique optical properties [21]. Prominent examples are the Lycurgus Cup (4th century AD), the glass of which contains small amounts of ~70 nm silver and gold NPs with 7:3 ratios, and the Maya blue paint (7th century AD) containing iron oxide NPs.

A large number of chemical synthesis routes have been employed for the fabrication of NPs with controlled morphology. Indeed, nanorods, nanocages and branched NPs can be synthesized [22–24]. NPs of different morphologies exhibit distinct optical responses due to the collective oscillations and localization of conduction electrons giving rise to LSPR modes. Regarding the chemical synthesis of NPs, the Brust [25] and the Turkevitch [26] aqueous preparation methods are usually employed for the production of NPs with diameters less than 10 nm and 10–40 nm, respectively. However, a ligand exchange step should be followed, in order to prevent aggregation during growth [27].

Another fascinating method for the production of surfactant-free NPs is the pulsed laser ablation of a solid target immersed in a liquid medium [28,29]. This technique is simple and has the advantage of producing a large variety of NPs that are free of both surface-active substances and counter-ions. Indeed, the absence of unnecessary reagents such as stabilizers and byproducts that are usually generated in chemical syntheses becomes useful when NPs are used for applications. On the other hand and contrary to chemical synthesis methods, using laser ablation in liquids it is
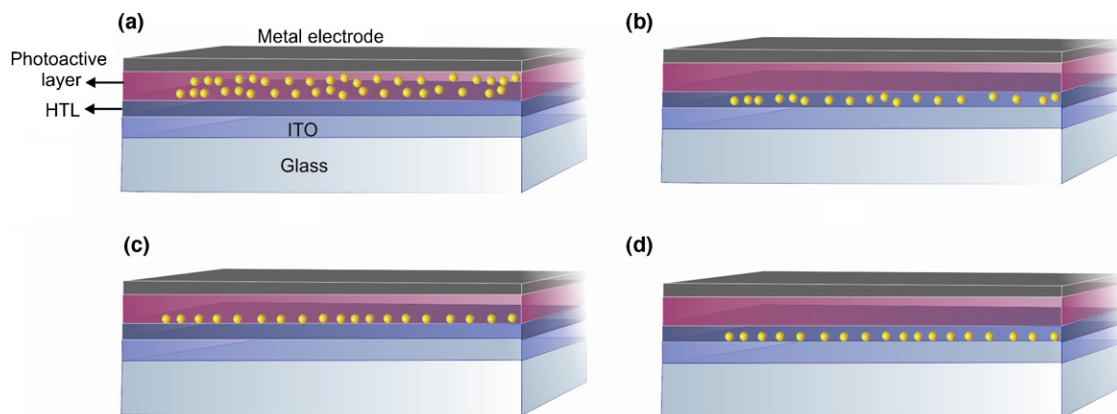

FIGURE 3

Schematic design of the different approaches for incorporating metallic NPs in bulk heterojunction OPVs. NPs (a) in the photoactive layer (b) in the hole transport layer (HTL) (c) at the HTL/photoactive layer interface and (d) at the ITO/HTL interface.

TABLE 1

Device characterization (efficiency n, relative efficiency change ± (%)) data of OPVs with NPs embedded in various configurations.

Geometry	Photoactive layer	η (%)	± (%)	Mechanism	Ref.
NPs dispersed into the active layer					
40 nm Ag clusters	PCDTBT:PC$_{70}$BM	6.45	16	Charge transport	[38]
	P3HT/PC$_{70}$BM	4.36	23		
70 nm Au NPs	PCDTBT:PC$_{70}$BM	7.1	13	Scattering	[39]
4.8–7.4 nm Au NPs	P3OT-C$_{60}$	1.9	73	Electrical	[31]
4.2–6.4 nm Ag NPs		1.65	50		
3.7 nm Au NPs	P3HT:PCBM	1.5	−67	Exciton quenching	[35]
20 nm Ag NPs	P3HT:PCBM	2.06	96	LSPR + morphology	[20]
110 nm Ag NWs	P3HT:PCBM	3.91	18	LSPR + scattering	[40]
Ag NPs		3.56	8		
5–15 nm Ag NPs	P3HT:PCBM	3.3	−3	Monomolecular recombination	[34]
Ag NPs	P3HT/PC$_{71}$BM	4.0	25	Scattering	[41]
Ag nanoplates		4.4	37		
40 nm Ag NPs	PCDTBT/PC$_{71}$BM	6.4	8		
200–500 nm Ag nanoplates		6.6	12		
1.5–20 nm Au NPs	P3HT:PCBM	3.71	41	LSPR + scattering + morphology	[36]
NPs dispersed into the hole transport layer (PEDOT:PSS)					
30–40 nm Au NPs	P3HT:PCBM	4.19	20	LSPR	[50]
45 nm Au NPs	P3HT:PCBM	4.24	19	LSPR	[53]
18 nm Au NPs	P3HT:PCBM	3.51	13	LSPR, hole collection	[51]
15 nm Au NSs	MEH-PPV:PCBM	2.36	19	LSPR	[54]
Au 55 nm NSs + 12 nm NRs	P3HT:PCBM	4.28	24	LSPRs	[58]
60 nm Ag NPs	P3HT:PCBM	2.75	64	LSPR	[56]
70–80 nm Au NPs in PEDOT (IL)	Tandem P3HT:IPCA–PSBTBT:PC$_{70}$BM	6.24	19	Strong local near-field	[57]
NPs dispersed between interfacing layers					
13 nm Ag NPs at the ITO/PEDOT:PSS interface	P3HT:PCBM	3.61	20	LSPR	[68]
1 nm thick Ag NPs film at the ITO/PEDOT:PSS interface	P3HT:PCBM	2.2	69	Plasmon	[69]
30 nm Au nanodots at the ITO/PEDOT:PSS interface	P3HT:PCBM	3.65	20	Plasmon	[72]
12.5 nm Ag NPs between ITO/PEDOT:PSS interface	P3HT:PCBM	2.82	17	Scattering	[70]
12.5 nm Ag NPs between active layer/Al		2.65	10	Resistance reduction	
110 nm Au NPYs (nanopyramids) at the ITO/PEDOT:PSS/interface	P3HT:PCBM	1.1	200	Near field plasmonic	[112]
5–10 nm Au NPs at the PEDOT:PSS/active layer interface	P3HT:PCBM	3.36	−8	Recombination	[66]
7–9 nm Au NWs (nanowires) at the ITO/PEDOT:PSS/interface	P3HT:PCBM	2.72	12	Far field scattering	[73]
40 nm Ag NTs (nanotriangles) at the ITO/PEDOT:PSS/interface	PCDTBT:PC$_{61}$BM	4.52	7	LSPR + scattering	[110]
NPs combinations					
18 nm Au NPs in PEDOT and 35 nm Au NPs in active layer	P3HT:PCBM	3.85	22	LSPR	[74]
50 nm Au NPs into the active layer and Ag grating with 750 nm period as back reflector	PBDTTT-C-T:PC70 BM	8.79	16	LSPR + SPP	[75]
40–50 nm Au and Ag NPs into the PEDOT:PSS layer	PTB7:PC70BM	8.67	20	LSPR	[76]
25 nm Au–Cu NPs alloy between the ITO and PEDOT:PSS layers	P3HT:PCBM	3.35	14	LSPR	[77]
10 nm Au-GO into PEDOT:PSS layer	P3HT:PCBM	3.55	10	LSPR	[78]
2D arrays of NPs					
Periodic Ag nanotriangle array on ITO	PCDTBT:PCBM	4.52	7	LSPR	[108]
Periodic Au nanopyramids on ITO	(P3):PCBM	1.1	205	LSPR	[109]

difficult to produce monodispersed colloids of NPs. Finally, traditional deposition techniques including, vapor-phase deposition, photo- and nanosphere lithography, electrodeposition, and thermal annealing have been employed to create various patterns of metal NPs on different layers within OPV devices.

Incorporation of NPs into the active layer

Solution processed NPs dispersed into the photoactive layer of OPV devices can significantly enhance the optical absorption, either via the formation of scattered waves at the large diameter NPs or due to the excitation of LSPR modes at the smaller diameter NPs [30]. Increased optical absorption is the result of stronger local optical fields in the vicinity of NPs that give rise to an enhanced exciton yield in single and multi-junction (tandem) OPV cells. The enhancement effect extends to wavelengths longer than the plasmon resonance wavelength for which the losses in the metallic NPs become insignificant. On the other hand, a third important process acting against the above light harvesting effects is the exciton recombination at the NP–blend interface, which should be minimized in order for the incorporation of the NPs to have a net positive effect on the PCE. In general, plasmonic device optimization is performed via tuning the NP material, including mixtures and alloys, geometric characteristics, such as size distribution and shape, as well as topological distribution within the solar cell architecture.

The first report on the addition of small amounts of metal NPs such as Au and Ag into the photoactive layer was by Kim and Carroll [31]. NPs had 5–6 nm diameters and were stabilized with a ligand shell of dodelcyl amine. A performance enhancement of more than 70% was mainly attributed to the introduction of dopant states in the active layer or the interfaces, which improves electrical conductivity and series resistance. The enhancement of absorption due to scattering was reported to be a minor effect.

There have been several reports indicating that the PCE shows a minute increase or even deteriorated upon the incorporation of chemically synthesized Au NPs into the active layer [32,33]. In this case the presence of surfactants and ligand coatings promotes undesirable exciton quenching, via nonradiative energy transfer between the NPs and the active layer, which decreases the plasmonic improvement effect. In particular, it has been shown that dodecylamine-capped Au NPs enable efficient quenching of excited states in the polymer [32]. In another investigation, it was shown that the addition of chemically synthesized Ag NPs in the active layer does not only enhance the local absorption, but it also leads to increased carrier mobility, since Ag NPs are more conductive than the active layer. However, the net conversion efficiency was not improved owing to the increased carrier recombination at Ag NPs acting as traps [34]. Finally, the effects of poly(ethylene glycol) capped Au NPs have also been investigated. It has been shown that the LSPR introduced by the metallic NPs enhances the light absorption in the active layer. However, the inferior electrical properties of NP-based blends compared to the NP-free ones give rise to a reduced overall performance improvement.

In order to prevent dispersed NPs acting as recombination centers, coatings of NPs with insulating materials was recommended [33]. Nevertheless, the plasmonic efficiency and thus absorption enhancement was shown to significantly deteriorate upon increasing the thickness of the insulating coating [35]. A promising solution proposed to mitigate the adverse effect of exciton quenching is the use of bare, uncoated NPs [36]. For this purpose, metallic NPs formed by laser ablation in liquids [28] that are free of surfactants and passivation layers [37], were used as additives in the active layer of OPV devices. It was demonstrated that the incorporation of surfactant-free Au NPs in the active layer can significantly enhance the device performance by 40% (Fig. 4(a)) attributed to LSPR and scattering effects. Indeed, the spectral range of IPCE (Incident Photon to Charge Carrier Efficiency) enhancement in Fig. 4(b), was found to comply with the theoretically predicted extinction spectra of Au NPs (Fig. 4(c)), suggesting that LSPR effects are primarily responsible for the efficiency enhancement. Besides this, the rather broad NPs size distribution obtained by the laser production process indicates the occurrence of scattering effects from the large diameter NPs. The use of surfactant-free NPs appears to be an efficient way to suppress exciton quenching via the elimination of recombination taking place on the capping layer of chemically synthesized NPs.

Improvements in OPVs efficiency due to enhanced scattering by large truncated octahedral 70 nm Au NPs [38], and 40 nm Ag NP clusters [39] embedded in a PCDTBT:PC$_{70}$BM photoactive layer have recently been reported with efficiency enhancements of 13% and 16%, respectively (Fig. 5). In case of Au NPs, the efficiency improvement was attributed to the enhanced light absorption due
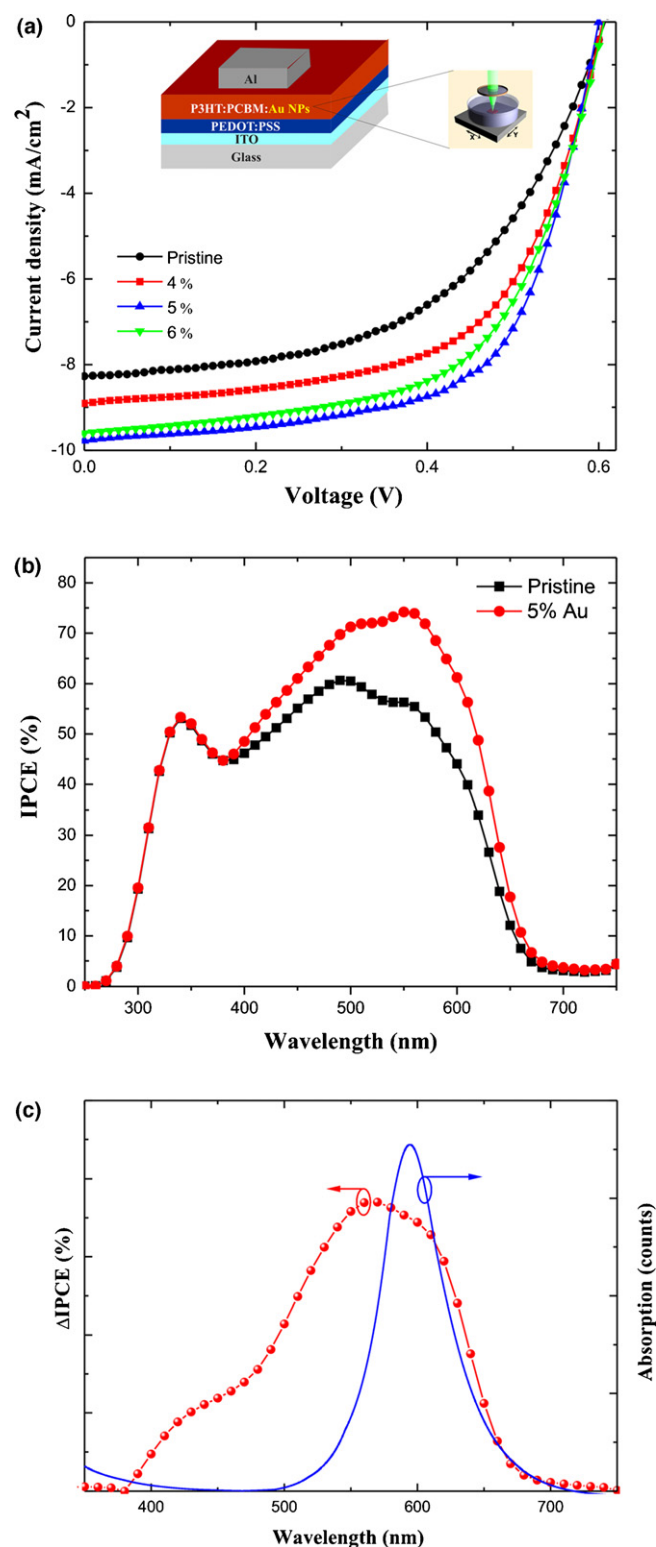

FIGURE 4

(a) J–V characteristics of the OPV devices with Au NPs embedded in the active layer. (b) Corresponding IPCE curves of these OPV devices. (c) Comparison between the curve of the increase in IPCE (ΔIPCE) after incorporating Au NPs and the calculated extinction spectrum of the Au NPs in the P3HT:PCBM medium. Reprinted with permission from Ref. [36] © 2012 American Institute of Physics.
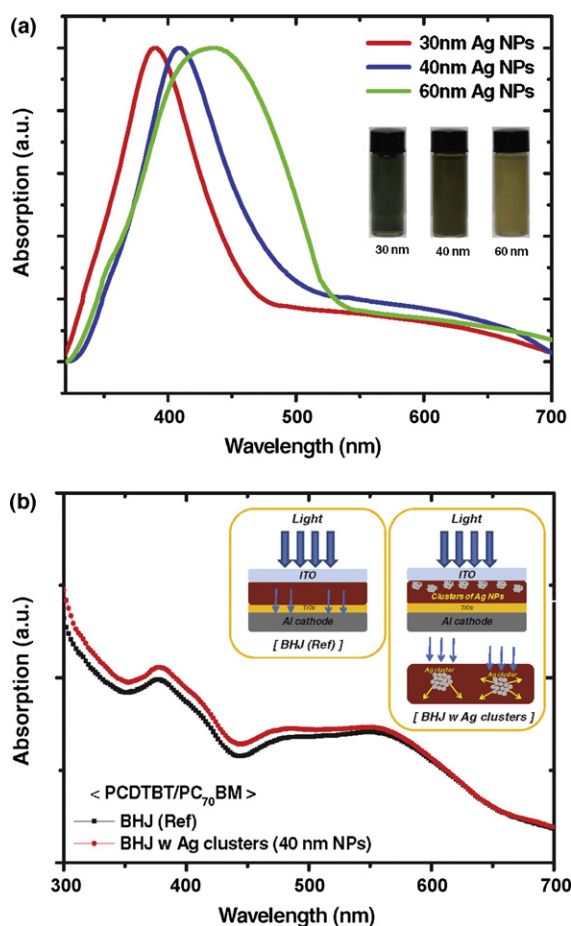
FIGURE 5

UV–Vis spectra of (a) Ag NPs of several diameters (30 nm, 40 nm, and 60 nm) (the inset figure shows Ag NPs of different colors dispersed in ethanol); (b) the plain PCDTBT/PC 70 BM BHJ film and the BHJ film with 40 nm-sized NP-based Ag clusters (1 wt%). The inset schematic figures show the light trapping and optical reflection by the scattering and excitation of LSPR. Reprinted with permission from Ref. [39] © 2011 John Wiley & Sons, Inc.

to scattering from NP LSPR modes. On the other hand, the improved charge transport was the reason for the enhanced efficiency of Ag NP-based OPV cells.

Finally, the NP shape is reported to influence the performance of plasmonic OPV cells. In particular, a direct comparison between Ag NPs and NWs was performed [40] with efficiency enhancements of 18% and 7.5%, respectively. Metallic NWs can provide greater enhancement than NPs due to improved electron transport exhibited by the respective devices [40]. In other work, the effect of NP shape has been investigated and Ag NPs were compared with Ag nanoplates as additives in P3HT-PC$_{71}$BM OPV devices. Results showed an efficiency enhancement of 25% and 37.5% for the NPs and nanoplates, respectively. The superiority of the nanoplates is attributed to their shape, which favors both efficient scattering and light trapping [41].

A different aspect on the influence of metallic NPs, recently demonstrated, is that the incorporation of NPs in the photoactive blend does not only lead to an increase in the performance but gives rise to enhanced structural stability of the blend [20]. This behavior can explain the observed disparity between the absorption and IPCE enhancement effects. In particular, the structural superiority of the photoactive layer with embedded Ag NPs was confirmed through an unconventional joint energy dispersion X-ray (EDXR) and Atomic Force Microscopy (AFM) analysis approach.

As shown in Fig. 6(a) and (b), experiments performed during illumination of the NP-free active layer revealed two major dynamical phenomena: a bulk reorganization process indicated by the increase of the active layer thickness over time and a degradation effect taking place at the interface between the active and the buffer PEDOT:PSS layers. On the contrary, the NPs-doped active layer exhibited only a minor aging effect taking place at the blend/PEDOT:PSS interface (Fig. 6(c)). Such improved morphological stability of the composite layer was further supported by electrical measurements under photodegradation, confirming that the NPs-based devices exhibited longer lifetimes. Finally, it was recently clarified that the improved stability against photodegradation of
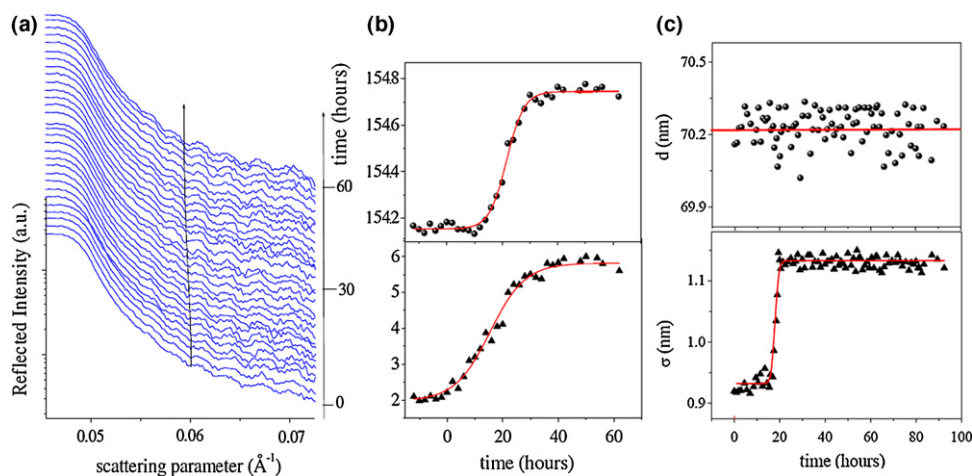

FIGURE 6

Results of the time-resolved EDXR study of the reference (NP-free) and doped with Ag NPs OPV devices: (a) the raw patterns as a function of the scattering parameter, q, and of illumination time, t, for the reference device. From these patterns the evolution over t of morphological parameters, such as the active layer thickness (d) and the roughness (σ) of the active layer/PEDOT:PSS interface, can be determined; (b) time evolution of d and σ for the reference sample; (c) time evolution of the same parameters for the NPs doped sample. Reprinted with permission from Ref. [20] © 2011 John Wiley & Sons, Inc.

plasmonic cells can be also ascribed to a NP-mediated mitigation of the photooxidation effect at the cathode/active layer interface. The NPs embedded into the blend act as quenchers of the triplet excitons and in this way the photooxidation process can be impeded [42].

The enhancement of the blend morphology was also confirmed in a recent study, where inorganic nanoparticles were embedded in the active layer of P3HT-PCBM OPV devices (Fig. 7) [43]. The spatially aggregated PCBM phase and organization of P3HT-related phases in the composite film were quantitatively characterized by using simultaneous grazing-incidence, small-angle and wide-angle X-ray scattering techniques. A performance enhancement of 55% was found upon the incorporation of NPs, attributed to a tuning of the phase-separated nanostructure of the active layer.

Theoretical simulations of metallic NPs dispersed in BHJ active layer can estimate the effect of different light trapping mechanisms in the respective conversion efficiency. In this concept, the absorption enhancement in OPVs induced by incorporating Al, Ag, and Au NPs into the active layer was modeled [35,44–46]. Finite element method simulations were employed to study the influence of Ag NPs on light absorption in P3HT:PCBM OPVs [35]. Indeed, absorption enhancements in the order of 1.5 for devices featuring an array of 23 nm diameter NPs with a spacing of 40 nm were predicted. Using a Finite Difference Time Domain method, the role of period, diameter and position of Ag NPs in enhancing the optical absorption of MEH-PPV:PCBM can be performed [47]. An, up to three-fold, increase in absorption is observed due to the

localized SPP and scattering [45]. The model was successfully extended to cases of mixed NP types. In addition, a recent study suggested that Al NPs have the potential to yield significantly greater enhancement than Ag or Au, due to the much higher plasma frequency of Al, which ensures a better overlap between plasmon resonance and the absorption band of organic semiconductors [44].

NPs into the HTL
Incorporation of NPs into the buffer PEDOT:PSS layer is one of the simpler methods of taking advantage of plasmonic effects. In this case, light-trapping can be achieved by scattering incident light at wide angles into the active layer. As a result, the light path length within the cell volume increases and may potentially lead to total internal reflection. It is also possible for this scattered light to excite SPPs on the back interface and other photonic modes into the active layer. However, the degree of contribution of LSPR effects remains inconclusive. In a recent study of the electrical and optical properties of OPVs with Au NPs embedded into the PEDOT:PSS layer, it was demonstrated that the performance enhancement was due to hole collection improvements and reduced exciton quenching, instead of LSPR effects [48]. Besides this, and similar to the effect of NPs embedded into the active layer, NPs induce morphological and/or chemical changes in the PEDOT:PSS layer [49]. Such morphological and/or chemical effects may contribute to the overall performance of OPVs incorporating NPs into or in contact with PEDOT:PSS.
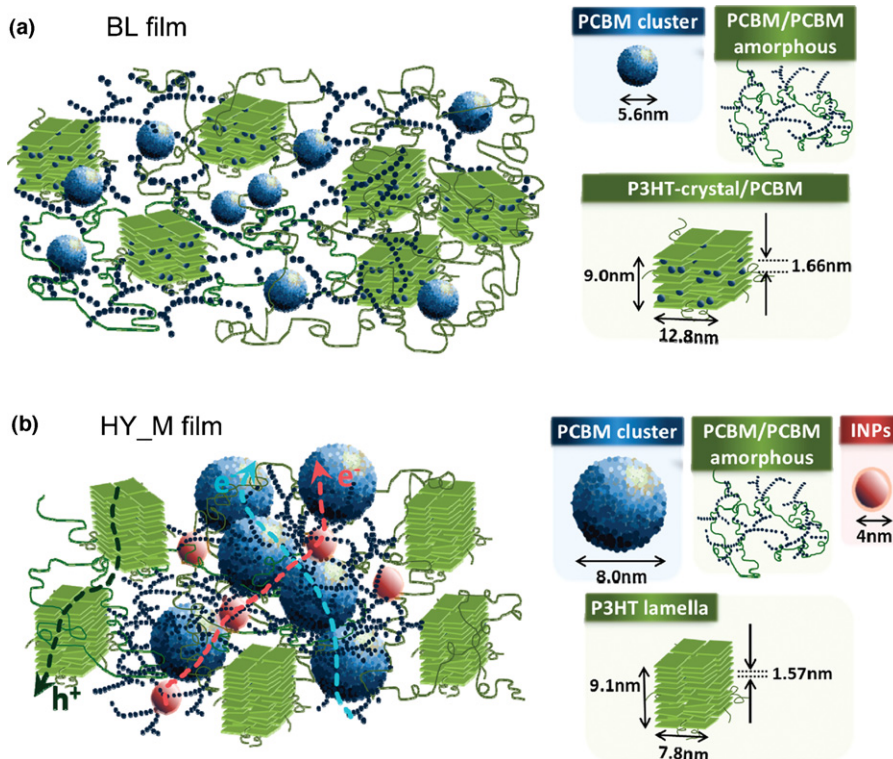

FIGURE 7

Schematic representation of the spatial arrangement of PCBM clusters, P3HT-crystal/PCBM domains, and the PCBM/P3HT amorphous domains in the phase-separated BHJ morphology of (a) P3HT/PCBM blended film (BL) and (b) P3HT/PCBM/Cu₂S inorganic nanoparticles (INPs) hybrid film (HY_M). The nanoparticle-tuned nanostructure in (b) provide a much more effective transport pathway through conventional interconnected PCBM clusters (light blue) or NP-containing network in the PCBM/P3HT amorphous domain coupled with interconnected PCBM clusters (light red). Reprinted with permission from Ref. [43] © 2012 American Chemical Society.

The first report on performance enhancement via the incorporation of Au NPs into the PEDOT:PSS layer was by Chen et al. [50]. The addition of Au NPs increased the exciton generation rate and the probability of exciton dissociation, thereby enhancing J_{sc} and fill factor (FF). An improvement of 20% was observed and was attributed to the local enhancement in the electromagnetic field due to the excitation of LSPR. More information was recently provided by Fung et al., who studied the electrical and optical properties of OPV cells with PEG-capped Au NPs embedded in the PEDOT:PSS layer [51]. It was shown that the absorption enhancement due to incorporation of Au NPs is insignificant and provides only a minor contribution to efficiency enhancement. This was postulated to be due to the lateral distribution feature of the strong near-field of plasmonic resonance around the metallic NPs. Considering electrical characteristics, they showed that the incorporation of an appropriate amount of Au NPs reduces the resistance of the PEDOT:PSS layer [48]. Moreover, there is an increase in the interfacial roughness between P3HT:PCBM and PEDOT:PSS after incorporation of Au NPs. The roughened interface contributes to the improvement of hole collection efficiency and leads to J_{sc} and FF enhancements.

In another relevant study, monodispersed octahedral 45 nm Au NPs, synthesized by a hydrothermal process [52], were blended in the PEDOT:PPS of P3HT:PCBM devices [53]. Steady state and dynamic photoluminescence (PL) measurements revealed interplay between the LSPR absorption enhancement and the LSPR induced reduction of exciton lifetime facilitated the charge transfer process. In this way an efficiency enhancement of 19% was observed.

The effect of size of chemically synthesized Au nanospheres (NSs) embedded in PEDOT:PSS was also investigated [54]. It was shown that the efficiency enhancement strongly depends on NP size. Furthermore, Au nanostructures of various sizes and shapes (nanospheres (NSs) and nanorods (NRs)) were mixed with the PEDOT:PSS buffer layer [55]. It was shown that the presence of a combination of NSs and NRs increased the efficiency by 24%. Since NSs and NRs exhibited different absorption bands, efficient light absorption as a result of LSPR and scattering effects was achieved (Fig. 8).

Besides this, Au NPs were successfully incorporated into a PEDOT:PSS film, which played the role of the interconnecting layer, which connects the two subcells in an inverted tandem OPV device. The addition of Au NPs improved both the top and bottom subcells' efficiency at the same time via LSPR enhancement of their optical absorption. As a result, a 20% improvement of efficiency was attained [56].

The causes of the improved optical absorption based on a cylindrical Ag-NP optical model, simulated with a 3D FDTD method were recently investigated. The model is able to explain the optical absorption enhancement due to LSPR modes, and provides a greater understanding of Ag-NP shape parameters that play a significant role towards determining broadband absorption phenomena in plasmonic OPVs. An increase of 60% was predicted, due to the strong optical field intensity associated with LSPR [57].

NPs at the interfaces

As mentioned before, in order to enhance the OPV performance using NPs, exciton quenching by nonradiative energy transfer between the active layer and the NPs must be minimized by state of the art control of the NP synthetic protocols. On the contrary, exciton quenching can be avoided when NPs are placed at the interfaces between the blend and ITO or the PEDOT:PSS layers. Through the incorporation of NPs at interfaces within OPVs it is possible to excite both LSPRs at their vicinity as well as SPPs along the intervening planar surfaces. Therefore, the role of the NPs is two-fold, namely to enhance absorption on the one hand and to collect charge carriers on the other.

In most reports incorporation of NPs at the various OPV interfaces is performed via dispersion from solution. The first report of placing Cu nanoclusters at the ITO–CuPc interface was reported by Stenzel et al. in 1995 [58]. A photocurrent enhancement by a factor of 2.7 was recorded. At that time, the enhancement was assigned to LSPR induced strengthening of the electric field. This argument was then turned around by Westphalen et al., who showed that the excited plasmons are capable of emitting electrons directly in a preferential direction, assuming that the NPs are placed inside an oriented electrical field [59]. However a breakthrough in the field took place in 2004, when Rand et al. incorporated Ag nanoclusters
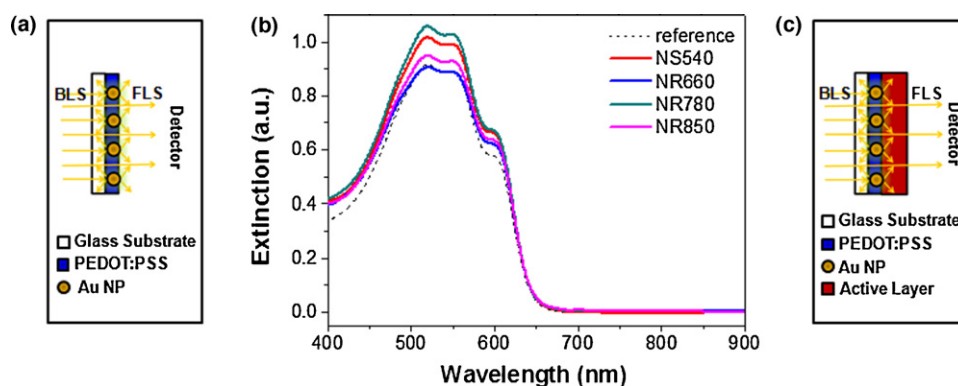

FIGURE 8

Schematic representation of two ways of enhancing light trapping of PEDOT:Au buffer layers through plasmonic (a) nanorods (NRs) and (c) nanospheres (NSs); (b) extinction spectra of devices on various PEDOT:Au NP buffer layer/glass substrates. The respective LSPR wavelengths of 540 nm for NS and 660, 780, and 850 nm for NR into the PEDOT:PSS buffer layer are indicated in the legend. Reprinted with permission from Ref. [55] © 2012 American Chemical Society.

as the intermediate layer in tandem OPV cells [60]. An efficiency enhancement by a factor of more than two was observed. It was shown that the optical field was enhanced by both LSPR and scattering supported by clusters. Later, Xue et al. used Ag nanoclusters in tandem cells based on two BHJs, resulting in 15% higher efficiency than the single cell [61].

Yoon et al. placed a self-assembled monolayer of Ag nanospheres between the PEDOT:PSS and the photoactive layer of P3HT:PCBM cells [62]. A photocurrent enhancement was recorded, mainly due to the LSPR-enhanced photogeneration of excitons. Although the measured photocurrent was increased, significant open-circuit voltage (V_{oc}) and FF losses were observed. This drawback can be explained by the possibility that Ag NPs act as an energy barrier for the charge extraction and injection. Kulkarni et al. showed that charge carrier generation could be enhanced more than three times if a thin film of Ag nanoprisms was introduced under the photoactive layer [63].

More recently, surfactant free Ag and Au NPs, produced by ultrafast laser ablation in liquids, were placed between the PEDOT:PSS and the photoactive layer interface [64]. An efficiency enhancement of 20% was obtained, mainly due to LSPR induced by the metallic NPs, which led to a noticeable enhancement of J_{sc}. The same approach was followed by Kymakis et al., utilizing carbon nanotubes as the transparent electrode, instead of ITO [65]. In another similar work, alkyl amine stabilized gold Au NPs with diameters of 1–10 nm, were deposited at the interface of the PEDOT:PSS and photoactive layers [66]. In contrast to the surfactant free NPs, the presence of organic stabilizing ligands at the interfacial layer minimizes the device performance. This result is in accordance with the case of adding NPs to the active layer and both highlight the importance of using uncoated NPs for plasmonic enhancement.

Another approach commonly used is the realization of irregular patterns of NPs between the various OPV interfaces either by employing different deposition techniques or by exploiting self-assembly methods. An interesting work, in this respect, is the thermal assisted deposition of a discontinuous thin Au layer between the photoactive P3HT:PCBM and the LiF buffer layers [67]. In this configuration, an efficiency enhancement of 30% was obtained. The photocurrent enhancement was ascribed to plasmon enhanced absorption due to the presence of a nanotextured Au layer. Relevant research followed with the placement of pulse-current electrodeposited uniform sized Ag NPs between the ITO electrode and the buffer PEDOT:PSS layer [68]. An efficiency enhancement of 20% was observed. Nevertheless, the highest efficiency enhancement of 70% was obtained with a 1 nm thin film of Ag NPs deposited by vapor phase deposition on the ITO electrodes [69]. In another interrelated work by Kalfagiannis et al., a direct comparison of the P3HT:PCBM OPV device performance with electron beam evaporated Ag NPs placed either between the ITO electrode and the PEDOT:PSS buffer layer or between the photoactive layer and the Al electrode was made [70]. NPs on top of the ITO led to better overall performance with an increased efficiency of 17%. Both light scattering and LSPR effects contributed to the improvement of the device performance. On the other hand, placing the NPs on top of the photoactive layer resulted in 25% higher efficiency. In this case, the enhancement was directly correlated with the better performance of the buffer layer through the reduction of its resistance.

Uniform Au NPs coated silanized ITO electrodes were fabricated by self-assembly [71] and employed in P3HT:PCBM OPV devices. An absorption and efficiency enhancement of 65% and 30%, respectively was observed in device structures with 20% NP surface coverage. In the same concept, Au nanorods were deposited onto the ITO electrode via layer-by-layer electrostatic assembly and transformed into nanodots through a thermally induced transition [72]. An efficiency increase of 20% was obtained, mainly due to the presence of the plasmon field in the vicinity of the nanodots. Another recent approach concerns the realization of Au NW networks (Fig. 9), based on solution-phase synthesis, as plasmonic antennae [73]. The reduction of the spacer layer thickness, which allows the evanescent field to be extended into the photoactive layer and the geometry of the Au-NW bands which favors the enhanced scattering collectively, resulted in an increased photocurrent by 23.2% and efficiency by 11.4%.

## Combination of NPs and/or NP configurations

NPs are found to have distinct mechanisms for improving device performance when incorporated in different positions within the solar cell architecture. To take advantage of this differential effect NPs were placed in two different configurations simultaneously [74]. For example, a 22% efficiency improvement was demonstrated by incorporating monofunctional poly(ethylene glycol) (PEG) Au NPs in both the hole transport and the photoactive layers of an OPV cell. In a similar manner dual plasmonic nanostructures, comprising a 1D back reflection Ag grating plus Au NPs embedded inside the active layer, were incorporated into small-bandgap BHJ cells [75]. A PCE increase from 7.59% to 8.79% was achieved. Broadband absorption enhancement was demonstrated, attributed to the simultaneous excitation of hybridized LSPRs from the Ag nanograting and Au NPs, respectively (Fig. 10).

Incorporation of mixed types of NPs is another approach that has been used for PCE improvement. In particular, Lu et al. reported on OPVs based on a cooperative effect of Ag and Au NPs. This concept led to the realization of BHJ PTB7:PC70BM OPV cells with a power conversion efficiency of 8.67%, accounting for a 20% net enhancement [76]. It is further demonstrated that the LSPR-induced local field enhancement also benefits charge separation and transport, resulting in increased charge carrier density and lifetime. Using a polystyrene-block-poly(2-vinylpyridine) copolymer template, arrays of an Au–Cu NP alloy have been fabricated between the ITO and PEDOT:PSS layers of OPVs [77]. It was found that, due to LSPR effects in bimetallic nanostructures, light absorption of the polymer thin layer was enhanced resulting in higher efficiency compared to conventional OPV cells.

Finally, in an effort to address the clustering and non-uniform dispersion drawbacks of solution processable plasmonic NPs, graphene oxide (GO) sheets have been utilized as a template to host NPs [78]. In particular, Au NPs adhered to GO sheets were blended into the PEDOT:PSS of BHJ OPVs. The GO template is found to be helpful on prohibiting aggregation of Au NPs and promoting the plasmonic effect without dramatically sacrificing the electrical properties.

Ordered arrays of plasmonic NPs

Although random dispersion of plasmonic NPs is simple and can be easily applied, it is quite challenging to control NP distribution
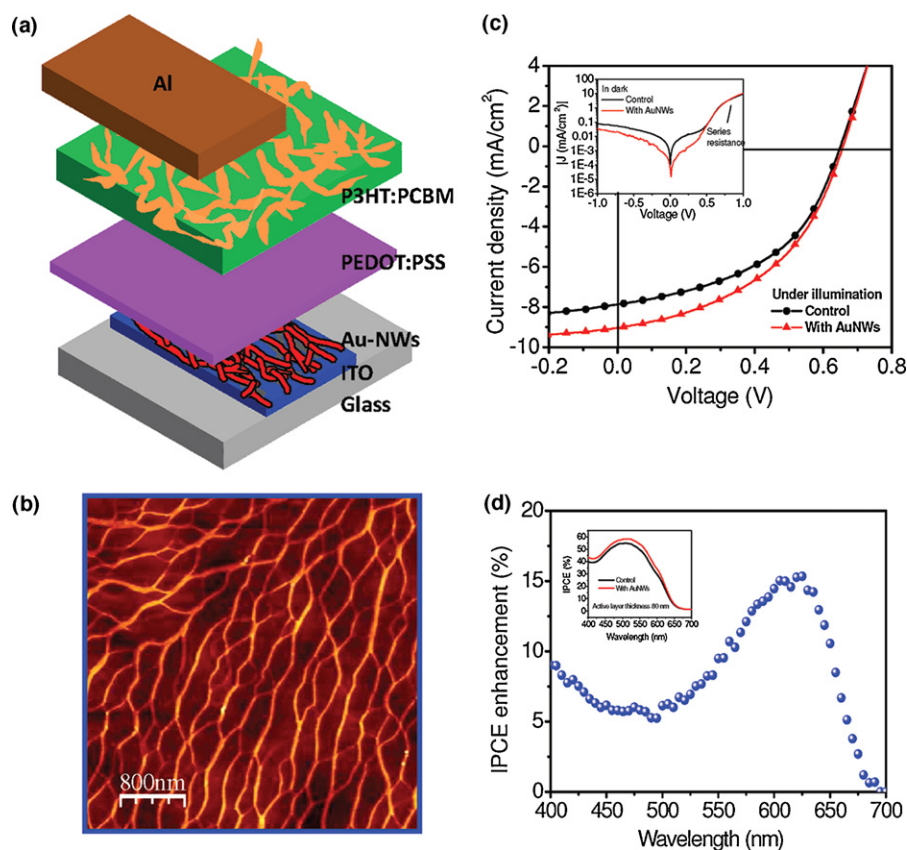
FIGURE 9

(a) Structure of an OPV cell incorporating NW networks at the interface between ITO and PEDOT:PSS layer. (b) Atomic force microscopy image of self-assembled Au-NW networks. (c) J–V characteristics of an 80 nm thick device with and without Au-NWs under illumination (100 mW/cm^2). The inset shows J–V curves of the same device in the dark on a semilog scale. (d) IPCE enhancement (%) in the 400–700 nm spectral range for the Au-NW integrated device with thickness 80 nm. The inset plot is IPCE spectra of the control and Au-NW incorporated devices. Reprinted with permission from Ref. [73] © 2012 American Chemical Society.

and topology within the OPV architecture. Notably, the random distribution of plasmonic NPs could lead to inhomogenous broadening effects and depending on the nature of NPs used, interaction and coupling between them and metal electrodes could negate any enhancement, leading to reduced PCE [79]. Crucial details necessary for device optimization may therefore be overlooked when using nonperiodic plasmonic NPs. In this respect, ordered arrays of periodically patterned metallic NPs offer a unique approach towards optimizing the optical absorption improvement and light-harvesting in OPVs [80]. Indeed, highly ordered arrays offer better tunability of the resonance spectral positions, the benefit of hosting additional, order-sensitive, electromagnetic modes [81], while being more suitable systems for theoretical simulation.

Light trapping via depositing ordered arrays in OPVs could in principle be achieved by exploiting two excitation geometries; namely plasmonic in-coupling of scattered light into the absorbing medium as well as coupling to propagating SPPs at the interface between the active layer and a metallic electrode, parallel to the device plane. In the latter case the electromagnetic energy transferred to SPPs promotes enhanced absorption in the active layer. However, ordered NPs arrays can also be used as an external layer for favorable plasmonic in-coupling of scattered light into the absorbing medium in solar cells [16]. In a typical configuration, NP arrays are deposited onto the front or back surface of the

solar cell, either embedded into the front or back electrode or electronically isolated by an intermediate transparent dielectric layer. Using proper designs of such 2D or quasi-3D arrays it is possible to excite waveguide modes which propagate in the active layer parallel to the device plane [82,83] (Fig. 11(a)–(d)). Alternatively, it is feasible to couple incident light to cavity modes, which propagate in a direction perpendicular to the device plane (Fig. 11(e)–(g)) [84,85]. Although the excitation of waveguide modes in dye-sensitized solar cells was demonstrated [86], to date there have been no reports on waveguide excitation using metallic NPs in OPVs. Theoretical simulations have provided some insight into the light coupling processes that can occur upon using NPs arrays [87].

Although 1D metallic nanogratings [88–92] have been explored in various OPV configurations to achieve improved performance, 2D periodic metallic nanopatterns exhibit superior plasmonic properties. Indeed, due to the polarization dependence of the 1D gratings, light trapping significantly differs between transverse-electric and transverse-magnetic modes. On the contrary, ordered 2D or quasi-3D patterns offer the possibility for simultaneous optimization of optical absorption for both polarization modes [93]. Besides polarization independence, 2D or quasi-3D arrays offer the possibility for broadband absorption enhancement over the entire visible and part of the near-infrared solar spectrum
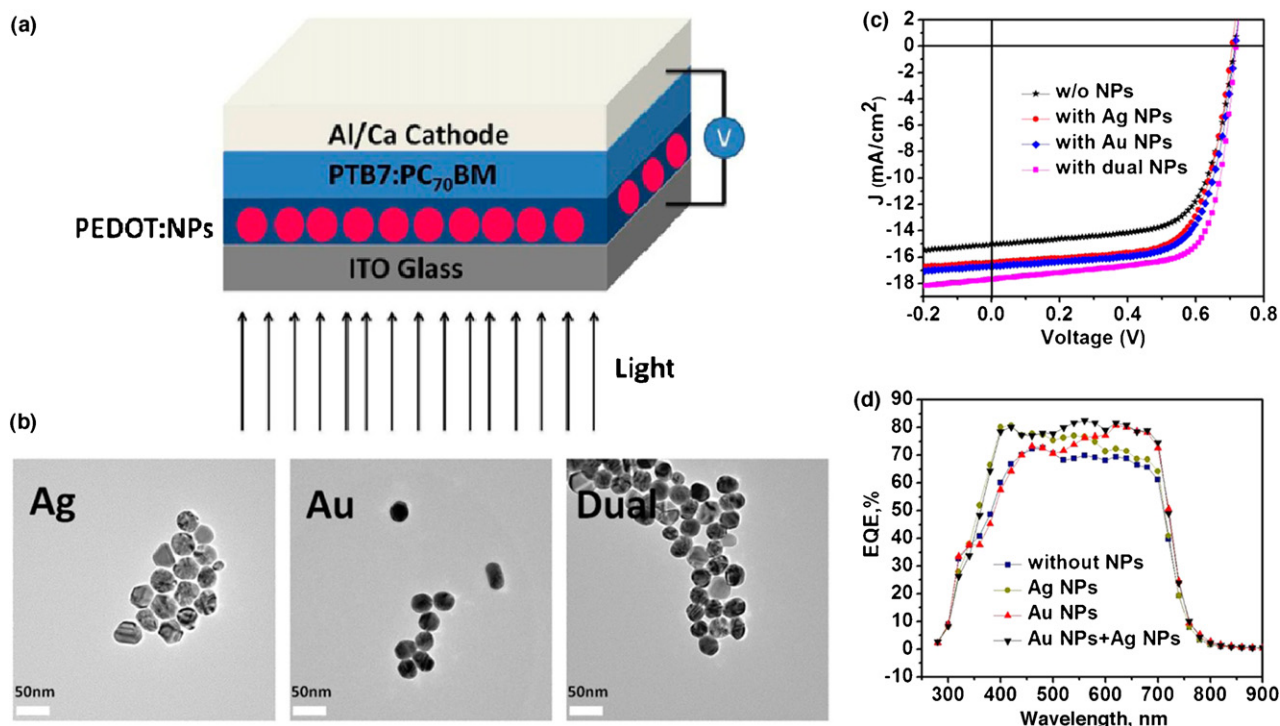
FIGURE 10

(a) Device structure of the solar cell incorporating mixed NPs of Au and Ag; (b) TEM images of Ag, Au, and dual NPs; (c) current−voltage characteristics of solar cells with and without NPs; (d) EQE spectra of PTB7/PC70BM with and without NPs. Reprinted with permission from Ref. [76] © 2012 American Chemical Society.
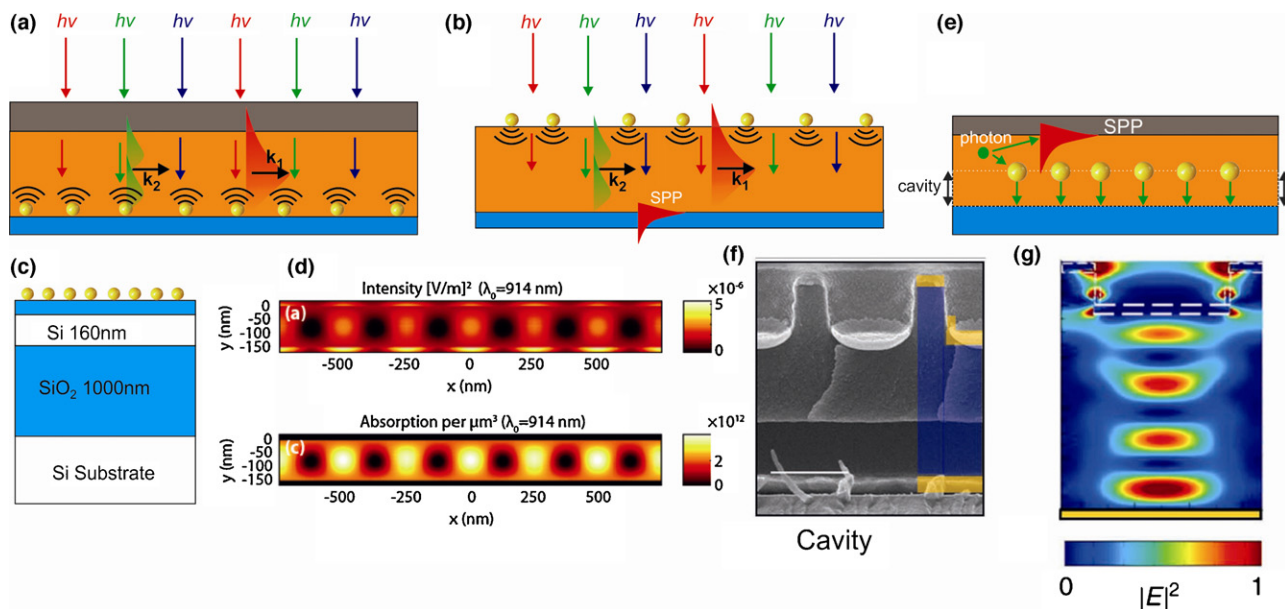

FIGURE 11

Alternate approaches for light trapping in solar cells using ordered arrays of plasmonic metallic NPs. Scattering of light into waveguide modes within a device, facilitated by ordered arrays of NPs on the back (a) or front side (b). (c and d) Example of a theoretical simulation for the excitation of a waveguide mode in a Si-based sample (however the same can be applied for a system where organic layers replace the inorganic ones): the sample used in the simulation is shown in (c), where the top blue layer is a 30 nm SiO_2 spacer layer and the particles are assumed to be silver spheres with $d = 300$ nm pitch. Part (d) shows cross sections of three unit cells of the waveguide (located between -160 nm $\leq y \leq 0$ nm in (c)) showing the intensity (top) and the absorption (bottom) profiles corresponding to light coupling to a waveguide mode propagating in the in-plane direction. (e) Schematic of scattering of light in cavity modes. (f) Cross-sectional SEM image of a cavity in a quasi-3D plasmonic crystal. (g) FDTD-computed cross-sectional intensity distribution for the cavity shown in (f). (d) From Ref. [83]. Reprinted with permission from Ref. [84] © 2011 Nature Publishing Group.

[94–97]. Indeed, randomly distributed NPs exhibit resonant frequencies within a narrow spectral band which poses a limitation for OPV applications. On the contrary, 2D periodic arrays of NPs [94] or combination of 2D NPs arrays with periodic nanopatterns and/or nanometric metallic mirrors [94,98–100] could potentially lead to an efficiency enhancement over a broad spectral range. Finally 2D periodic metallic nanopatterns could be employed to address the angular tolerance limitation exhibited by conventional plasmonic nanostructures. Indeed, owing to the dispersive nature of plasmonic modes the SPP resonant absorption peak position depends substantially on the incident light angle giving rise to significant absorption losses. Research on this topic led to various angle-insensitive architectures in the visible and near-IR spectral region including, omnidirectional absorbers [101–103], plasmonic black bodies [104] 2D periodic metallic nanopatterns [105,94], and metamaterials structures [106]. However, the influence of most of them on the OPV performance has not yet been investigated and could be an interesting topic for future research.

Several 2D periodic NPs configurations have been employed to enhance the efficiency of OPVs. Zhu et al. demonstrated a plasmonic nanostructure design by embedding a layer of hexagonal periodic metallic nanospheres between the active layer and transparent anode of BHJ OPVs (Fig. 12(a)) [97]. Such a hybrid structure demonstrated a broadband optical absorption enhancement from LSPR with a weak dependence on the polarization of the incident light. Diukman et al. showed an increase in the external quantum efficiency of OPV cells after embedding ordered arrays of Au NPs extending into the active layer [79]. Two enhancement mechanisms were identified, namely enhanced absorption driven by LSPR and that driven by a cavity mode of a circular nano patch antenna. In another study, blue-ray disk recordable substrates are used as the diffraction grating structures on which silver films are deposited by vacuum evaporation. P3HT:PCBM films were subsequently spin-coated on silver/grating substrates [107]. Up to a two-fold increase in the short-circuit photocurrent is observed when the LSPR modes are excited on the gratings. More recently, large area plasmonic 2D periodic Ag or Au nanotriangle arrays (Fig. 12(b)) fabricated by nanosphere lithography were incorporated in BHJ OPV devices based on PCDTBT:PCBM [108], and silole–thiophene (P3):PCBM [109] active layers, respectively. PCE enhancements from 4.24% to 4.52%, 0.36–1.1% and 0.6–1.2% were reported, respectively.

The incorporation of 2D periodic plasmonic arrays into OPVs has been also theoretically investigated. In particular, an array of Al nanodisks was placed at the interface of the ITO anode and the active layer, forming circular plasmonic nano-patch cavities between the nanodisks and the Al electrode that sandwiches the active layer [110] (Fig. 12(c)). With this configuration, absorption enhancements of up to 40% were observed in a device integrated with an array of nanodisks with a diameter of 100 nm and a periodicity of 250 nm. Based on theoretical considerations, a pioneer device structure was proposed by Ren et al., through incorporation of patterned Ag NPs on top of the ITO electrode with a conductive optical layer inserted between the photoactive and the back metal electrode layers [111]. In this way, a striking and broadband enhancement of the photoactive layer absorption is achieved, resulting in a photocurrent enhancement of 1.67.

Bai et al. were the first to propose that the combination of 2D nanopatterns gives rise to an efficient polarization-independent,
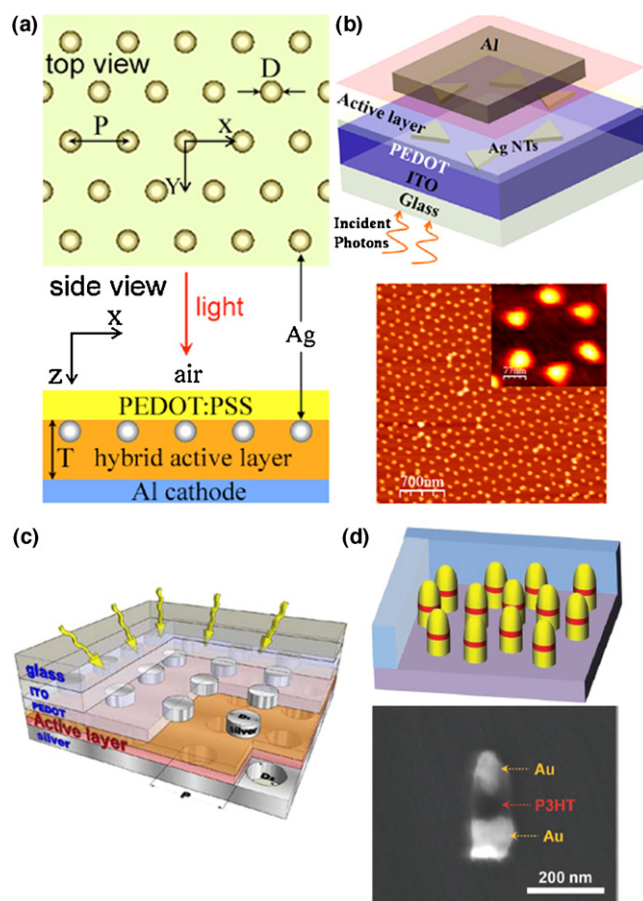

FIGURE 12

Examples of novel plasmonic architectures based on 2D ordered arrays of NPs incorporated into BHJ OPVs and respective absorption or PCE enhancements: (a) plasmonic nanospheres array. (b) Plasmonic nanotriangle array. (c) Thin-film double plasmonic nanostructure OPV with nanodisks and nanoholes placed next to the electron donor- (CuPc) and electron acceptor (PTCBI) layers, respectively. (d) Vertically oriented gold-P3HT-gold nano-antenna arrays and a single element. (a) Reprinted with permission from Ref. [97] © 2011 American Institute of Physics. (b) Reprinted with permission from Ref. [108] © 2012 American Chemical Society. (c) From Ref. [99]. (d) Reprinted with permission from Ref. [112] © 2011 John Wiley & Sons, Inc.

broadband absorption enhancement in OPV cells. In particular a double plasmonic structure design comprising a 2D periodic array of Au nanodisk on top and a nanopatterned Ag nanohole array on the bottom interface of the active layer was introduced [99]. Excitation of coupled modes of localized SPPs at the nanodisks and short-range SPPs at the nanohole array gives rise to a significantly enhanced electromagnetic field within the organic active layer. Indeed, theoretical calculations showed that an optimized double plasmonic structure can enhance the total photon absorption by >125% for molecular OPVs. However, experiments measuring the performance of OPV devices incorporating such hybrid plasmonic structures should be performed to test the above theoretical predictions.

Most recently, O'Carroll et al. reported on a novel array of metal–polymer–metal split-dipole nanoantennas, fabricated using a template-directed sequential electrodeposition process followed by a metal evaporation step [112] (Fig. 12(d)). The aim was to enhance the radiative emission rate and luminescence quantum

efficiency of P3HT sandwiched between the nanogap of the two 2D arrays of Au nanorods forming the nanoantennas. It was shown that the resonant scattering response of the entire antenna can be tuned to the P3HT emission band by controlling the nanoantenna length (Fig. 12(d)).

Summary and future outlook

The development of low-cost scalable processes that enable light-trapping in organic photoactive layers represents an important milestone toward a wider implementation of OPVs, since it can give rise to a prominent increase in device efficiency and stability and, in turn, to a reduction in the average cost/kW generating capacity of the technology. Incorporation of plasmonic nanostructures into OPV cells offers several unique features for efficient light management and constitutes the most promising strategy for the realization of this goal. If this approach of combining nanophotonics and photovoltaics is applied to state of the art OPV systems with today's record efficiency (i.e., 9.2% and 10.7% PCE for single [113] and tandem cell (www.nrel.gov/ncpv/images/efficiency_chart.jpg), respectively, an efficiency of 15% can be reached. This will be achieved by facile NP incorporation for enhanced optical absorption, and hence exciton generation of the OPV devices, without influencing the device architecture.

In this context, an in-depth understanding of the different enhancement mechanisms with respect to interrelationships between the properties of the NPs (nature, size, shape, distribution) with the performance parameters is more than essential. This development should be supported by extensive theoretical modeling, providing guidelines for the different NP parameters. Additional challenges will involve reaching the required parameters determined from simulation through NP synthesis and functionalization. Emphasis should also be given on controlled methodologies for incorporating these NPs into the cell (coating as a separate layer, mixing with the donor–acceptor solution, polarity, solubility, etc.). Furthermore, the use of NPs of various sizes and shapes and with different LSPR bands can be hierarchically placed in the form of single or multiple layers into the OPV devices, with the aim of optimizing the match between the device absorption and the solar spectrum. Besides this, the use of multi-junction or tandem devices with multiple bandgaps, in which NPs with different LSPR bands are placed into different polymer active layers and/or the interfaces, provides simultaneous benefits and has the potential to further enhance the conversion efficiency. Finally, photodegradation stability issues, which can also be addressed via NP incorporation into the active layer, should not be ignored [114].

Although the optical properties and the subsequent improvement in light-harvesting have mostly been the focus of studies to date, the electrical properties of NP-based OPVs are rather complex and revealing their exact role on solar cell performance remains a challenge. In this respect, careful consideration must be given for the type of NP used to avoid misalignment at the electronic band level which can introduce charge trapping states and therefore a reduction in the J_{sc} and degradation in the V_{oc} which is directly derived from the HOMO-LUMO levels of the donor and acceptor materials. Research on the optical properties of plasmonic OPVs should always be performed in conjunction with an investigation of the respective electrical properties.

In addition, there are many reports on large performance enhancements in non-optimized plasmonic devices, contrary to smaller improvements observed upon incorporation of NPs into state of the art OPVs. This clearly demonstrates that the NPs improve the performance via both plasmonic and morphology effects. In a high efficiency OPV morphology is well optimized, thus the contribution of the NPs on the structural and morphological properties is minor. In the case of a non-optimized device, both effects could be important. Furthermore, as pointed out above, the role of NPs on the electrical properties is still unclear. Therefore, the direct correlation of the photovoltaic characteristics with the optical, electrical and morphological properties of plasmonic devices, aiming at the quantification of the contribution of different NP-mediated mechanisms, will be a vital advancement.

Current research efforts are concentrated on the application of novel 2D as well as 3D plasmonic nanostructures to pursue further enhancement through efficient light trapping. Nevertheless, the primary challenge for the use of such systems is the fabrication cost that should be kept reasonably low for potential commercialization. Therefore, low-cost and large area nanofabrication techniques need to be developed and are highly desirable. Implementation of such emerging techniques for photon management may bring the vision of OPV commercialization closer to reality.

References

[1] F.C. Krebs, et al. Energy Environ. Sci. 3 (2010) 512.
[2] S.R. Forrest, Nature 428 (2004) 911.
[3] S.H. Park, et al. Nat. Photon. 3 (2009) 297.
[4] L.D. Dou, et al. Nat. Photon. 6 (2012) 180.
[5] C.E. Small, et al. Nat. Photon. 6 (2012) 115.
[6] V. Shrotriya, et al. Appl. Phys. Lett. 88 (2006) 064104.
[7] G. Dennler, et al. Adv. Mater. 21 (2009) 1323.
[8] E.T. Yu, J. van de Lagemaat, MRS Bull. 36 (2011) 424.
[9] H.A. Atwater, A. Polman, Nat. Mater. 9 (2010) 205.
[10] W.L. Barnes, et al. Nature 424 (2003) 824.
[11] C.F. Bohren, D.R. Huffman, Absorption and Scattering of Light by Small Particles, Wiley-Interscience, New York, 1983.
[12] S. Pillai, et al. Sol. Energy Mater. Sol. Cells 94 (2010) 1481.
[13] K.L. Kelly, et al. J. Phys. Chem. B 107 (2003) 668.
[14] T. Jensen, et al. J. Cluster Sci. 10 (1999) 295.
[15] W.E.I. Sha, et al. Appl. Phys. Lett. 99 (2011) 113304.
[16] S. Pillai, et al. J. Appl. Phys. 101 (2007) 093105.
[17] F.J. Beck, et al. Opt. Express 19 (2011) A146.
[18] J. Weickert, et al. Adv. Mater. 23 (2011) 1810.
[19] W.E.I. Sha, et al. Opt. Lett. 36 (2011) 478.
[20] B. Paci, et al. Adv. Funct. Mater. 21 (2011) 3573.
[21] L.M.L. Liz-Marzán, Mater. Today 7 (2004) 26.
[22] M. Iqbal, et al. J. Mater. Chem. 17 (2007) 335.
[23] B. Lim, Y. Xia, Angew. Chem. 50 (2011) 76.
[24] H.A. Day, et al. Cryst. Eng. Commun. 12 (2010) 4312.
[25] M. Brust, et al. Chem. Commun. 7 (1994) 801.
[26] J. Turkevich, Gold Bull. 18 (1985) 86.
[27] C.J. Ackerson, et al. J. Am. Chem. Soc. 127 (2005) 6550.
[28] G.W. Yang, Laser Ablation in Liquids, Pan Stanford Publications, 2012.
[29] E. Stratakis, et al. Opt. Express 17 (2009) 12650.
[30] J.-Y. Lee, P. Peumans, Opt. Express 18 (2010) 10078.
[31] K. Kim, et al. Appl. Phys. Lett. 87 (2005) 203113.
[32] K. Topp, et al. J. Phys. Chem. A 114 (2010) 3981.
[33] M.D. Brown, et al. Nano Lett. 11 (2011) 438.
[34] M. Xue, et al. Appl. Phys. Lett. 98 (2011) 253302.
[35] H. Shen, et al. J. Appl. Phys. 106 (2009) 073109.
[36] G.D. Spyropoulos, et al. Appl. Phys. Lett. 100 (2012) 213904.
[37] E.V. Barmina, et al. Quant. Electron. 40 (2010) 1012.
[38] D.H. Wang, et al. Angew. Chem. 50 (2011) 5519.
[39] D.H. Wang, et al. Adv. Energy Mater. 1 (2011) 766.
[40] C.-H. Kim, et al. ACS Nano 5 (2011) 3319.

[41] D.H. Wang, et al. RSC Adv. 2 (2012) 7268.
[42] B. Paci, et al. Nanoscale 4 (2012) 7452.
[43] H.-C. Liao, et al. ACS Nano 6 (2012) 1657.
[44] V. Kochergin, et al. Appl. Phys. Lett. 98 (2011) 133305.
[45] N. Lagos, et al. Appl. Phys. Lett. 99 (2011) 063304.
[46] S. Vedraine, et al. Sol. Energy Mater. Sol. Cells 95 (2011) S57–S64.
[47] D. Duche, et al. Sol. Energy Mater. Sol. Cells 93 (2009) 1377.
[48] D.S. Dixon, et al. J. Mater. Chem. 21 (2011) 16349.
[49] M. Stavytska-Barba, et al. J. Phys. Chem. C 115 (2011) 20788.
[50] F.-C. Chen, et al. Appl. Phys. Lett. 95 (2009) 013305.
[51] D.D.S. Fung, et al. J. Mater. Chem. 21 (2011) 16349.
[52] C.C. Chang, et al. Chem. Mater. 20 (2008) 7570.
[53] J.-L. Wu, et al. ACS Nano 5 (2011) 959.
[54] L. Qiao, et al. Appl. Energy 88 (2011) 848.
[55] Y.S. Hsiao, et al. J. Phys. Chem. C 116 (2012) 20731.
[56] J. Yang, et al. ACS Nano 5 (2011) 6210.
[57] R.S. Kim, et al. Opt. Express 20 (2012) 12649.
[58] O. Stenzel, et al. Sol. Energy Mater. Sol. Cells 37 (1995) 337.
[59] M. Westphalen, et al. Sol. Energy Mater. Sol. Cells 61 (2000) 97.
[60] B.P. Rand, et al. J. Appl. Phys. 96 (2004) 7519.
[61] J. Xue, et al. Appl. Phys. Lett. 85 (2004) 5757.
[62] W.-J. Yoon, et al. Sol. Energy Mater. Sol. Cells 94 (2010) 128.
[63] A.P. Kulkarni, et al. Nano Lett. 10 (2010) 1501.
[64] G.D. Spyropoulos, et al. Photon. Nanostruct. 9 (2011) 184.
[65] E. Kymakis, et al. IEEE Trans. Electron Dev. 58 (2011) 860.
[66] H. Liu, et al. Sol. Energy Mater. Sol. Cells 96 (2012) 302.
[67] X. Chen, et al. Appl. Phys. Lett. 93 (2008) 123302.
[68] S.-S. Kim, et al. Appl. Phys. Lett. 93 (2008) 073307.
[69] A.J. Morfa, et al. Appl. Phys. Lett. 92 (2008) 013504.
[70] N. Kalfagiannis, et al. Sol. Energy Mater. Sol. Cells 104 (2012) 165.
[71] S. Shahin, et al. Appl. Phys. Lett. 101 (2012) 053109.
[72] J.H. Lee, et al. Org. Electron. 10 (2009) 416.
[73] T.Z. Oo, et al. J. Phys. Chem. C 116 (2012) 6453.
[74] F.-X. Xie, et al. Appl. Phys. Lett. 99 (2011) 153304.
[75] X. Li., et al. Adv. Mater. 24 (2012) 3046.
[76] L. Lu, et al. Nano Lett. 13 (2013) 59.
[77] M. Heo, et al. Adv. Mater. 23 (2011) 5689.
[78] G.-Q. Fan, et al. J. Mater. Chem. 22 (2012) 15614.

[79] I. Diukman, et al. Opt. Express 19 (2011) A64.
[80] C. Battaglia, et al. ACS Nano 6 (2012) 2790.
[81] S.H. Lim, et al. J. Appl. Phys. 105 (2009) 073101.
[82] R.A. Pala, et al. Adv. Mater. 21 (2009) 3504.
[83] J. van de Groep, Light trapping in thin silicon waveguides by plasmon mediated mode coupling, Research project for the masters degree in Nanomaterials: Chemistry and Physics at Utrecht University, The Netherlands, 2011
[84] D. Chanda, et al. Nat. Commun. 2 (2011) 479.
[85] N.C. Lindquist, et al. Appl. Phys. Lett. 93 (2008) 123308.
[86] Y.G. Wei, et al. Nano Lett. 10 (2010) 2092.
[87] V.E. Ferry, et al. Nano Lett. 8 (2008) 4391.
[88] C. Min, et al. Appl. Phys. Lett. 96 (2010) 133302.
[89] Y. Liu, et al. Appl. Phys. Lett. 101 (2012) 233904.
[90] X.H. Li, et al. J. Phys. Chem. C 116 (2012) 7200.
[91] J. You, et al. Adv. Energy Mater. 2 (2012) 1203.
[92] R. Zhu, et al. Adv. Mater. 23 (2011) 4193.
[93] W. Bai, et al. Opt. Express 18 (2010) A620.
[94] N. Liu, et al. Nano Lett. 10 (2010) 2342.
[95] A.E. Ostfeld, D. Pacifici, Appl. Phys. Lett. 98 (2011) 113112.
[96] S. Xiao, N.A. Mortensen, Opt. Lett. 36 (2011) 37.
[97] J. Zhu, et al. Appl. Phys. Lett. 98 (2011) 151110.
[98] H. Shen, B. Maes, Opt. Express 19 (2011) A1202.
[99] W. Bai, et al. J. Photon. Energy 1 (2011) 011121.
[100] J.N. Munday, H.A. Atwater, Nano Lett. 11 (2011) 2195.
[101] P. Spinelli, et al. Nat. Commun. 3 (2012) 692.
[102] J. Zhang, et al. Appl. Phys. Lett. 98 (2011) 261101–261111.
[103] A. Abass, et al. J. Appl. Phys. 109 (2011) 023111–23121.
[104] V.G. Kravets, et al. Phys. Rev. B 78 (2008) 205405.
[105] T.V. Teperik, et al. Nat. Photon. 2 (2008) 299.
[106] M.K. Hedayati, et al. Adv. Mater. 23 (2011) 5410.
[107] N. Baba, et al. ACS Appl. Mater. Int. 3 (2011) 2080.
[108] B. Wu, et al. J. Phys. Chem. C 116 (2012) 14820.
[109] A. Kirkeminde, et al. Nanoscale 4 (2012) 4421.
[110] B. Wu, et al. Plasmonics 7 (2012) 667.
[111] W. Ren, et al. Opt. Express 19 (2011) 26536.
[112] D.M. O'Carroll, et al. Adv. Mater. 24 (2012) OP136.
[113] Z. He, et al. Nat. Photon. 6 (2012) 593.
[114] E. Stratakis, et al. Nanoscale (2013), http://dx.doi.org/10.1039/C3NR00656E.